Article

Design and test of a student hybrid rocket engine with an external carbon fiber composite structure

Francesca Heeg [1,†,*], **Lukas Kilzer** [1,†], **Robin Seitz** [1] **and Enrico Stoll** [1,]

[1]   Institute of Space Systems (IRAS), Technische Universität Braunschweig (TUBS), 38108 Braunschweig, Germany.

*   Correspondence: f.heeg@tu-braunschweig.de; Tel.: +49-531-391-95951

†   These authors contributed equally to this work.

Abstract: The development of hybrid rockets offers excellent opportunities for the practical education of students at universities due to a high safety and a relatively low complexity of the rocket propulsion system. During the German educational program STERN, students of the Technische Universität Braunschweig obtain the possibility to design and launch a sounding rocket with a hybrid engine. The design of engine HYDRA 4X is presented and results of first engine tests are discussed. Results for measured regression rates are compared to results from literature. Furthermore, the impact of the lightweight casing material CFRP on the hybrid engine mass and flight apogee altitude is examined for rockets with different total impulse classes (10 to 50 kNs). It is shown that the benefit of a lightweight casing material on engine mass decreases with an increasing total impulse. However, a higher gain on apogee altitude, especially for bigger rockets with a comparable high total impulse is shown.

Keywords: hybrid rocket engine; sounding rocket; carbon fiber composite; engine test; total impulse; lightweight design

---

1. Introduction

Hybrid rocket propulsion systems offer several advantages compared to solid or liquid propulsion, such as operational safety, thrust throttling ability and lower cost due to a simple system design, as stated in [1] and [2]. However, several drawbacks prevented the achievement of an advanced technical readiness level (TRL) in the past [3], which hindered the establishment of hybrid propulsion systems in the commercial space market [4]. One disadvantage of hybrid propulsion is a low fuel consumption rate, called regression rate, that can lead to a low thrust density and sometimes complex fuel grain shapes [5]. Another challenging aspect is the inconstant oxidizer to fuel mass ratio during operation. It is caused by the fuel grain surface that changes with continuing fuel consumption [6]. These disadvantages offer a wide range of research potential, hence, various aspects of hybrid rocket engines (HRE) are addressed in respective research. One of the main parameters under research is the experimental characterization of fuel regression rate as investigated in [2,7,8] and how it is linked to heat transfer in the combustion chamber [9]. The regression rate also depends on other parameters like propellant choice [10,11] and oxidizer injecting system [12,13]. Other aspects like throttling, combustion modeling or design optimization are investigated in [14], [15] and [16] respectively. Due to the advantages of HRE, they are suitable for a variety of space applications such as space launch systems [1], upper stages [17], lunar and mars ascent stages [5,18] and sounding rockets especially for university education. Hence, there are numerous activities of hybrid rocket engine development at universities around the globe. For example, Tsohas et al. [19] describe the 4 kN hybrid rocket development and launch at Purdue University, where the engine is propelled with hydrogen peroxide

(H_2O_2) and low density polyethylene (LDPE). At Tokai University, Japan, students develop engines with a thrust of up to 600 N that is achieved by using a propellant combination of nitrous oxide (N_2O) and wax-based fuel [20]. Meanwhile, the Stratos hybrid rockets that are developed by team DARE of Technical University Delft use a fuel combination of sorbitol, paraffin and aluminum powder. The engine DHX-200 Aurora of rocket Stratos II+ reaches a thrust of 10 kN and a total impulse of 100 kNs [21]. In Germany, the hybrid rocket activities of student groups have been expedited by a national educational program called Studentische Experimental-Raketen (STERN) that was initiated by the German Aerospace Center (DLR) Space Administration in 2012 and is funded by the Federal Ministry of Economic Affairs and Energy (BMWi) [22]. This program allows students from German universities to develop and launch a supersonic sounding rocket [22]. The students are familiarized with processes and reviews of a real aerospace project. The primary objectives of the rockets comprised a minimum altitude of 3 km, a minimum velocity of Mach 1 and the equipment with an onboard data transmission and a recovery system for a safe landing. During the project, the student teams were continuously supervised by experts in the field (Rocket propulsion (DLR Trauen, DLR Lampoldshausen) and DLR Mobile Raketenbasis (MORABA)) and the DLR Space Administration [23]. The participating student teams were able to launch their individual rockets from ESRANGE Space Center, Sweden [24]. Several of them used a hybrid propulsion system for their rockets, like the team of Hochschule Bremen. The rocket AQUASONIC used a N_2O/polyethylene (PE) engine to reach an altitude of about 6.5 km [24]. The HyEnD team of Universität Stuttgart developed the rocket HEROS that also used N_2O as oxidizer but in combination with paraffin as fuel. This engine shows a design thrust of 10 kN and an total impulse of over 100 kNs [24]. Also, the team of Universität Bremen contributed to the STERN program. They developed the rocket ZEpHyR, that applied an engine with liquid oxygen (LOX) and paraffin as propellants and achieved a total impulse of 54 kNs.

Another contribution to the program was made by the student association called ExperimentalRaumfahrt-InteressenGemeinschaft e.V. (ERIG), on behalf of Technische Universität Braunschweig. The students were able to successfully develop and launch the sounding rocket Faust in 2015, which used a hybrid rocket engine [23]. Due to the success and the excellent opportunity for practical education of university students, the STERN program was continued in a second phase since 2017 as STERN II. The rocket Faust II shall be developed as a successor of Faust, where the hybrid rocket engine shall be improved regarding performance and lightweight design. The design, main characteristics and performance of the Faust engine HYDRA 3X (HYbridDemonstrations-RaketenAntrieb) is described in the following. Based on this, the design changes for the advanced engine HYDRA 4X, which will propel Faust II rocket, are examined in detail, before first engine test results are presented. Measured regression rates are compared to results from literature. Furthermore, a detailed analysis of the impact of two different engine casing materials are discussed. Finally, conclusion and outlook on the effects of the new engine construction on lightweight design and rocket performance are presented.

2. Materials and Methods

2.1. Overview of sounding rocket educational project within STERN program

The main objective of the STERN program is the provision of experience for students in overall system design. A complete rocket system is to be designed with different subsystems to achieve the project requirements. This includes ground segment design, system operation design, project planning and documentation. An overview of the whole project content is presented in Figure 1. Various subsystems of the rocket are addressed within the flight segment. This is also shown in Figure 2, where the rocket subsystems are visualized. One main subsystem is the propulsion system, where the engine and valve and feeding systems are designed. The engine design and verification is emphasized in this article.
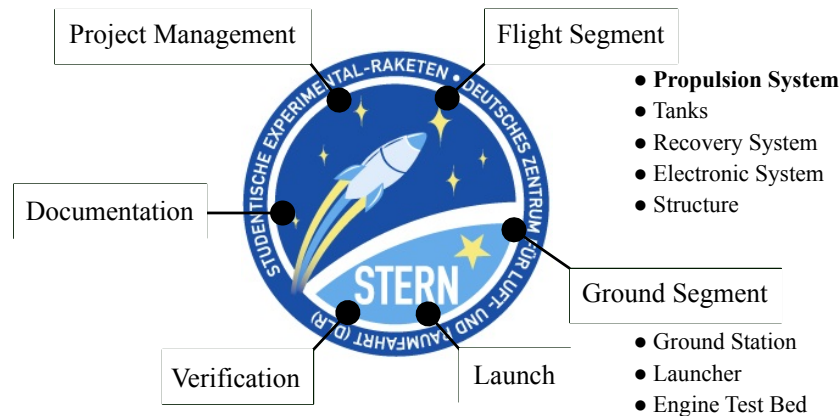
Figure 1. Overview of STERN II project contents (STERN program logo [22])

2.2. Design of Faust rocket and HYDRA 3X engine

Faust is a sounding rocket, which is propelled by a hybrid rocket engine. A schematic of the rocket is shown in Figure 2 and its main characteristics are listed in Table 1. Faust has a modular design of eight segments. The nose cone is part of the two-staged recovery system that is located on top of the electronics section. The complete propulsion system consists of a pressure vessel for pressurization of the oxidizer vessel, valves, feeding lines, and the hybrid engine. Fins for flight stability are connected to the body tube that accommodates the engine [25]. A successful launch with a maximum altitude of 5400 m was performed in 2015.
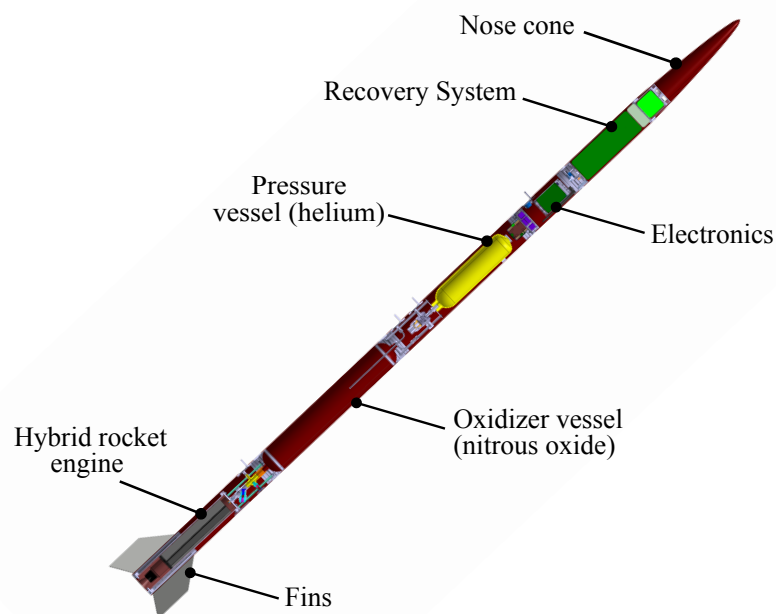

Figure 2. Design of the sounding rocket Faust

A hybrid engine was chosen for the Faust rocket because of the advantages of the propulsion concept. The operational safety is suitable for a student project and the propellants are storable and relatively safe to use. The hybrid engine HYDRA 3X uses a propellant combination of liquid N_2O as oxidizer and a solid mixture of 70 % hydroxyl-terminated polybutadiene (HTPB) and 30 % aluminum powder as fuel [26]. The aluminum was added to increase the fuel regression rate. Engine test runs with HYDRA 3X showed an increase in regression rate of about 20 % compared to tests without the addition of aluminum powder [26]. The engine design shows typical components of a hybrid engine, such as an

Table 1. Faust rocket characteristics

Parameter	Value
Diameter	0.12 m
Length	3.2 m
Mass	24.1 kg
Altitude	5410.5 m
Engine	HYDRA 3X

injector for feeding and vaporizing oxidizer into the following combustion chamber ([27]). It is based on a shower-head injector that additionally uses a cone for diverting the oxidizer to ensure a better distribution of the mass flow. The propellant fuel is cast directly into the combustion chamber, which uses a star-shaped mold for creating the required fuel geometry that is presented in Figure 3. The fuel grain ends at the vortex disk that generates a large vortex flow. This provides the required mixture of both propellants. Subsequently, a conical convergent-divergent nozzle is located at the end of the engine [26,28,29].
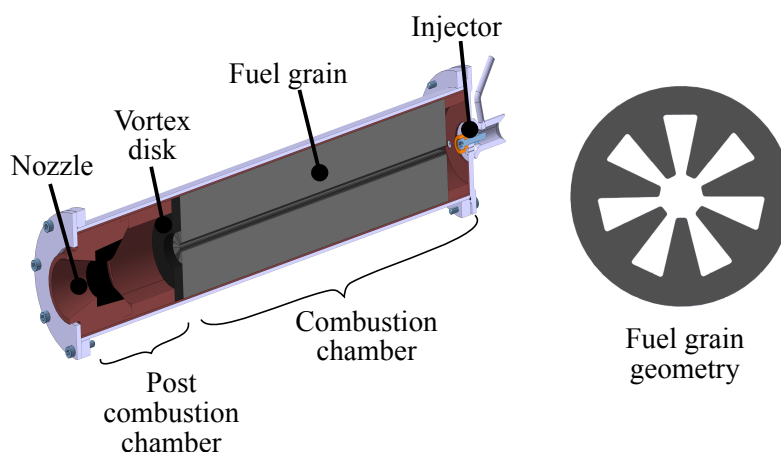
Figure 3. Design of engine HYDRA 3X

Most parts of the engine structure are manufactured from phenolic paper due to advantageous ablative cooling characteristics. The nozzle throat is additionally reinforced with graphite to withstand high thermal loads during combustion. The engine is encapsulated by a steel casing for resistance of combustion pressure loads. The engine outer diameter is 0.09 m and therefore smaller than the rocket diameter. Hence, an additional structure tube is necessary that is added to the engine casing mass. Structural and performance data of HYDRA 3X are given in Table 2. A successful flight of the Faust rocket was performed with the HYDRA 3X engine. It burned for 10 s with a mean thrust of 1.25 kN. After 37 s flight time an apogee altitude of 5.4 km was reached [23]. The following objectives for Faust II engine, HYDRA 4X, within the STERN II project were chosen:

- Apogee altitude of 10 km
- Increased engine thrust and total impulse
- Improved engine power to mass ratio
- Integrated lightweight casing made from carbon fiber reinforced plastic (CFRP)

2.3. Design of hybrid rocket engine HYDRA 4X

After the successful application of the HYDRA 3X engine, the HYDRA 4X engine for the Faust II propulsion system was planned. It uses pure HTPB as fuel, waiving additional aluminum powder. This propellant is cast into the engine at a liquid state. It cures by using hardener and therefore gets solid. The grain geometry is created by using a casting mold that is removed after the curing process.

The structure parts are made from phenolic paper while the nozzle throat is additionally supported with graphite. The structure must be able to withstand the combustion pressure loads. Thus, the engine is equipped with a CFRP laminate coating that resists the operational pressure. The injector head is based on the design of HYDRA 3X. It is a shower-head injector with channel orifices of 0.8 mm. A diverting cone is added as shown in Figure 4b. The oxidizer flow impinges on this cone that diverts the flow and directs it to the fuel grain. The current design of HYDRA 4X is presented in Figure 4a and key data in Table 2, respectively.
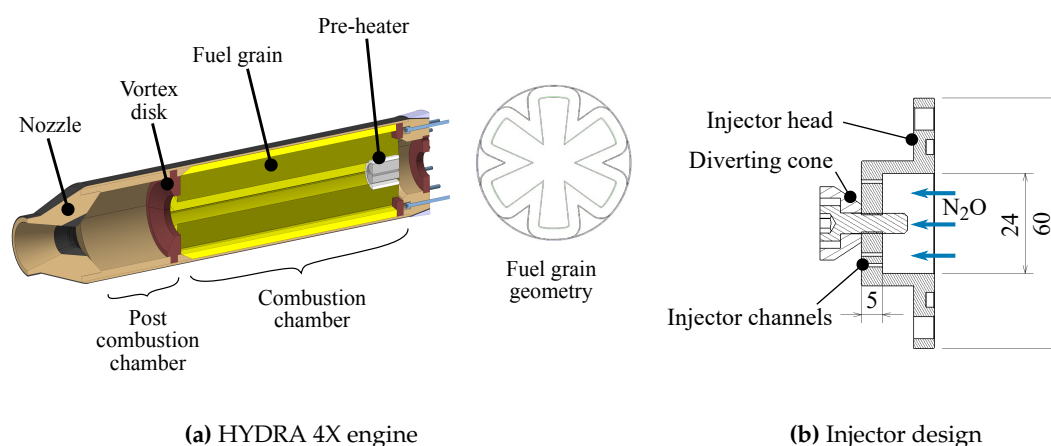

(a) HYDRA 4X engine   **(b)** Injector design

Figure 4. Design of HYDRA 4X engine and injector with injector channels and diverting cone

Table 2. Structural and performance characteristics of engines HYDRA 3X and 4X

Parameter	Symbol	HYDRA 3X	HYDRA 4X
Overall length	l	0.47 m	0.62 m
Overall diameter	d	0.09 m	0.14 m
Fuel grain length	l_f	0.31 m	0.34 m
Post combustion chamber length	l_{post}	0.05 m	0.10 m
Nozzle throat diameter	d_t	0.02 m	0.03 m
Nozzle area ratio	A_e / A_t	5.06	4.97
Mass	m	5.7 kg	5.78 kg
Fuel Mass	m_f	1.2 kg	2.57 kg
Casing Mass	m_{cas}	3.8 kg	0.31 kg
Thrust	F	1.25 kN	2.25 kN*
Total Impulse	I_{tot}	12.5 kNs	35.55 kNs*
Chamber Pressure	p_c	3 MPa	2.5 MPa *

*design value

2.4. Performance calculations

The technical design of the HYDRA 4X is built upon a first evaluation of an ideal ratio of N_2O and HTPB for a maximum specific impulse. NASAs CEA-Code (Chemical Equilibrium with Applications) suggests an oxidizer to fuel mass ratio of $O/F = 7$, using input data from Table 3 with a frozen composition assumed after the nozzle throat. The O/F is used to calculate combustion characteristics for the combustion chamber pressure and nozzle exit pressure. Since the ambient pressure of the rocket changes with altitude, a value for nozzle exit pressure needs to be defined. In this case, the nozzle is adapted to ambient pressure at half of the maximum flight altitude. Input data and relevant results of CEA are shown in Table 3.

Based on former flight tests experience, a lift-off acceleration of around 5 g should be achieved to ensure a reliable launch. This is the boundary condition to determine the required thrust F and thus, mass flow $\dot{m}$. This results in a thrust of 2.25 kN for the overall rocket mass of 46 kg. From

Table 3. Input data and results of CEA calculation

Parameter	Symbol	Value
Input parameter		
Oxidizer to fuel mass ratio [-]	O/F	7
Combustion chamber pressure [MPa]	p_c	2.5
Nozzle exit pressure [MPa]	p_e	0.085
Output parameter		
Temperature (chamber) [K]	T_c	3358.1
Molar mass of reaction product (chamber) [g/mol]	M	26.534
Ratio of specific heats (chamber) [-]	γ_c	1.1494
Ratio of specific heats (throat) [-]	γ_t	1.1474
Ratio of specific heats (exit) [-]	γ_e	1.2274
Specific impulse [m/s]	$I_{sp,CEA}$	2391.9

$$\dot{m} = \frac{F}{\eta_{engine} \cdot I_{sp,CEA}} \tag{1}$$

[1] and

$$\dot{m}_f = \frac{\dot{m}}{O/F + 1} \tag{2}$$

the required fuel mass flow $\dot{m}_f$ can be calculated. A global engine efficiency of $\eta_{engine} = 91\%$ was determined via engine tests during the first STERN program. This is a preliminary design assumption. Different star-shaped fuel grain geometries were iterated regarding number of star spikes and shape. A constant regression, perpendicular to the fuel grain geometry over full burn time was assumed. The regression rate for the preliminary design is approximated to $\dot{r} = 0.6\,\text{mm/s}$ from previous measurements of HYDRA 4. It was adapted with every hot fire test of HYDRA 4X for the design iteration. The mean regression rate of a hot fire test was obtained through weighing the engine before and after the test. The weight difference is converted into a geometric regression, by dividing the weight difference with burn time and fuel grain surface area prior to testing. An optimization was carried out for burn time t_b, thrust profile according to burn time and initial mass flow levels, given by Equation 2. This leads to a star shaped fuel grain with parameters shown in Figure 7a and Table 6. Using fuel grain geometry and mass flow $\dot{m}_f$, the O/F-ratio determines the subsequent oxidizer mass flow $\dot{m}_{ox}$:

$$\dot{m}_{ox} = O/F \cdot \dot{m}_f. \tag{3}$$

The propulsion system of Faust II is designed to inject liquid oxidizer into the engine. A pressure of $5\,\text{MPa}$ is chosen for pressurization of the oxidizer vessel. This pressure level ensures a liquid state of the nitrous oxide and thus operational temperatures up to $293\,\text{K}$ [30]. This temperature agrees with ambient temperature requirements set by a planned launch from ESRANGE Space Center. With combustion chamber pressure p_c and oxidizer vessel pressure p_{ox}, the theoretical injection speed v_{th} can be calculated using the oxidizer density ρ_{ox}, assuming incompressible, stationary, and isentropic Bernoulli flow (cf. [1]):

$$v_{th} = \sqrt{\frac{2}{\rho_{ox}}(p_{ox} - p_c)} \tag{4}$$

A diameter of $0.8\,\text{mm}$ and a length of $5\,\text{mm}$ were chosen for a single injector orifice. The volume flow $\dot{Q}$ in a single circular orifice is decreased compared to its theoretical optimum due to stream tube contraction and pressure losses within the orifices [6]. This relation can be expressed by

$$\frac{\dot{Q}}{\dot{Q}_{th}} = \frac{\dot{Q}}{v_{th}\frac{\pi}{4}d^2} = C_D \tag{5}$$

where the effects can be combined in a single factor C_D. This coefficient is measured in every test to iterate the number of injecting orifices. Equation 4 is only applicable to negligible changes of density along the injecting orifice length. Due to the strong temperature and pressure dependency, this is only partially applicable to nitrous oxide injection with a strong pressure gradient from feeding line to combustion chamber present. However, this approach was used in combination with the coefficient C_D to approximate the real flow behavior of the nitrous oxide.

The total number of injecting orifices n_{ox} can be calculated by

$$n_{ox} = \frac{\dot{m}_{ox}}{\rho_{ox} \cdot \dot{Q}} \tag{6}$$

The strong temperature and pressure dependency of the N_2O density ρ_{ox} and its effect on the number of injector orifices is to be handled with special consideration. A good control of the N_2O parameters during fueling can circumvent off-design engine operation. This is also achieved by varying the number of injector orifices according to N_2O parameters.

An auxiliary function Γ is introduced in Equation 7 [7]. The mean of specific heat ratios γ calculated by CEA in Table 3 are used as input. The characteristic velocity C^* and the throat area A_t are calculated by Equation 8 using molar mass M, temperature T_c of the reaction product in the chamber (cf. Table 3) and universal gas constant R_∞ [7]. Subsequently, the nozzle throat diameter d_t is computed in Equation 9.

$$\Gamma = \sqrt{\gamma} \cdot \left(\frac{2}{\gamma+1}\right)^{\frac{\gamma+1}{2\cdot(\gamma-1)}} \tag{7}$$

$$C^* = \frac{1}{\Gamma_c}\sqrt{\frac{R_\infty}{M} \cdot T_c} = \frac{p_c \cdot A_t}{\dot{m}} \tag{8}$$

$$d_t = \sqrt{\frac{4}{\pi} \cdot A_t} \tag{9}$$

The momentum thrust coefficient C_F^0 can be calculated according to Equation 10 by using the nozzle exit pressure p_e [7]. Equation 7 and Equation 10 are combined to the nozzle expansion ratio A_e/A_t in Equation 11 [7]. A conical nozzle is chosen due to simplicity in manufacturing. The divergence cone half angle is set to $15°$. The length of the divergent nozzle l_{nozzle} is calculated through Equation 12.

$$C_F^0 = \Gamma \cdot \sqrt{\frac{2 \cdot \gamma}{\gamma-1} \cdot \left[1 - \left(\frac{p_e}{p_c}\right)^{\frac{\gamma-1}{\gamma}}\right]} \tag{10}$$

$$\frac{A_e}{A_t} = \frac{\Gamma^2}{C_F^0 \cdot \left(\frac{p_e}{p_c}\right)^{\frac{1}{\gamma}}} = \frac{d_e^2}{d_t^2} \tag{11}$$

$$l_{nozzle} = \frac{d_e - d_t}{2} \cdot \frac{1}{\tan(15°)} \tag{12}$$

The thrust coefficient C_F is computed by Equation 13, applying a correction factor to the momentum thrust coefficient C_F^0, correcting for the axial divergence of the exhaust of a conical nozzle [1]. The ambient pressure p_a corresponds to static pressure of the environment and is equal to p_e at the design point. For following test data, the ambient pressure is measured at the test site.

$$C_F = C_F^0 \cdot \frac{1 + \cos(15°)}{2} + \frac{A_e}{A_t} \cdot \frac{p_e - p_a}{p_c} \tag{13}$$

Note that this corresponds to an optimum C_F achievable for conical nozzles.

The combustion η_c and nozzle expansion efficiency η_{nozzle} of the engine are calculated by Equation 14 and Equation 15 as ratios of experimentally measured parameters to ideal design values. This approach enables a comparison of actual engine performance with design performance. As the parameters might shift in the hot fire test, all experimental values are taken as mean over full burn time. According to [1], the overall engine efficiency is then calculated by Equation 16. All design data of HYDRA 4X engine in its latest iteration after the fourth hot fire test is summarized in Table 4.

$$\eta_c = \frac{C^*_{exp}}{C^*} = \frac{p_c \cdot A_t}{C^* \cdot (\dot{m}_{ox} + \dot{m}_f)} \tag{14}$$

$$\eta_{nozzle} = \frac{C_{F,exp}}{C_F} = \frac{F}{C_F \cdot p_c \cdot A_t} \tag{15}$$

$$\eta_{engine} = \frac{I_{sp,exp}}{I_{sp}} = \eta_{nozzle} \cdot \eta_c \tag{16}$$

Table 4. Design data of HYDRA 4X

Parameter	Symbol	Value
Oxidizer pressure [MPa]	p_{ox}	5
Combustion chamber pressure [MPa]	p_c	2.5
Mean density N_2O [kg/m^3]	ρ_{ox}	915.85
Discharge coefficient [-]	C_D	0.497
Orifice diameter [mm]	-	0.8
Orifice length [mm]	-	5
Mass flow oxidizer [kg/s]	$\dot{m}_{ox}$	0.93
Injector orifices [-]	n	55
Density HTPB [kg/m^3]	ρ_f	936.0
Regression rate [mm/s]	$\dot{r}$	0.72
Mass flow fuel [kg/s]	$\dot{m}_f$	0.13
Outer diameter fuel grain [m]	d_f	0.13
Length fuel grain [m]	l_f	0.34
Burn time [s]	t_b	15.8
Nozzle exit pressure [MPa]	p_e	0.085
Nozzle area ratio [-]	A_e/A_t	4.97
Momentum thrust coefficient [-]	C_F^0	1.47
Characteristic velocity [m/s]	C^*	1607
Throat diameter [m]	d_t	0.0295
Divergent nozzle length [m]	l_{nozzle}	0.07

3. Description of engine test bed

All engine tests are performed at the test facility of DLR Trauen, where all safety requirements can be achieved. The engine test bed for HYDRA 4X consists generally of two assemblies, the fluid supply system and the test bench. A schematic of the fluid supply system is presented in Figure 5a. The fluid supply system also includes the test bed electronics. An intermediate tank is used to store liquid N_2O during the fueling process. Nitrous oxide is fed from cylinders directly into this tank where it can be pressurized to 6 MPa. In contrast to the rocket system, nitrogen is used for pressurizing the N_2O tank on the test bed due to its better availability. Temperature and pressure within the intermediate tank are measured by three sensors. Strain gauges measure the tank weight during testing to control fueling and to determine oxidizer mass flow rates. After pressurization, the tank weight is set to zero. Thus, only the fueled nitrous oxide mass is measured. During the hot test, the intermediate tank is continuously pressurized by nitrogen. The change of tank weight during the hot test gives the oxidizer mass flow. The continuously added nitrogen mass flow for pressurization introduces a systematic

error to the oxidizer mass flow measurement during the hot test. The additional weight of the nitrogen decreases the measured oxidizer mass flow. This systematic error is not corrected. Hence, all stated oxidizer mass flows are smaller than to be expected.

The oxidizer feeding line is mounted to the test bench and leads directly to the test injector. Liquid N_2O is inserted into the engine through this component during hot test. At this point, additional measurements are taken: Temperature and pressure shortly in front of the injector are measured as well as the combustion chamber pressure by a sensor connected to a small pipe that leads directly into the engine pre-chamber. Pressure is measured at a sampling rate of 1 kHz. The test bench is a robust steel construction that is modular and can be used for different engines, as is displayed in Figure 5b. The HYDRA 4X is mounted to the test bench using a mounting plate, which accommodates the injector and can easily be exchanged. Four load cells are integrated onto the test bench for thrust measurement. Data logging and valve controlling is realized by National Instruments cRIO-9074 controller [29]. It is located within an electronic box near the fluid supply system and can be controlled remotely from the test control center.

4. Results and discussion

4.1. hot fire tests and iteration of design

The results for the first four hot fire tests of HYDRA 4X engine are presented in the following. Design changes have been made to increase engine performance between these tests. The changes of defined design parameters are summarized with the resulting measured values from corresponding hot fire tests in Table 5. The value G_{ox} is computed according to [7]

$$G_{ox} = \frac{\dot{m}_{ox}}{A_p} \tag{17}$$

where A_p is the free port area of the fuel grain. The mean port area over burn time is considered for determination of the regression rate.

Table 5. Overview of design and measured parameters of HYDRA 4X-01 to HYDRA 4X-04

Design parameter	H4X-01	H4X-02	H4X-03	H4X-04
Fuel grain geometry	Geometry v1	Geometry v1	Geometry v2	Geometry v2
Injector	36 orifices	40 orifices	40 orifices	55 orifices
Post combustion chamber length	0.06 m	0.09 m	0.1 m	0.1 m
For fuel grain geometries cf. Figure 7a				
Measured parameter as mean over burn time				
t_b [s]	8	15.7	12.2	12.3
F [kN]	1	1.2	1.6	2.3
p_c [MPa]	1.5	1.8	2	2.3
$\dot{m}_f$ [kg/s]	0.08	0.1	0.13	0.12
$\dot{r}$ [mm/s]	0.44	0.63	0.72	0.66
p_{ox} [MPa]	4.4	4.2	4.95	4.6
$\dot{m}_{ox}$ [kg/s]	0.72	0.63	0.65	1.01
G_{ox} [g/cm^{2}s]	15.7	10	10.7	17.2
O/F [-]	8.75	6.3	5	8.4

Pressure values of intermediate tank, injector and combustion chamber are measured during all engine tests. The measurements of the first four engine tests are presented in Figure 6. Three general test phases are visible in all four graphs: The first phase describes the condition when the intermediate N_2O tank is filled and pressurized to a pressure between 4.8 and 5.6 MPa. The combustion phase starts with opening of the main oxidizer valve and the tank pressure reduces slightly as oxidizer flows into the engine. A decrease of tank pressure over time can be noticed. This is a result of an insufficient pressurization of the used fluid supply system, which was originally designed for lower oxidizer mass
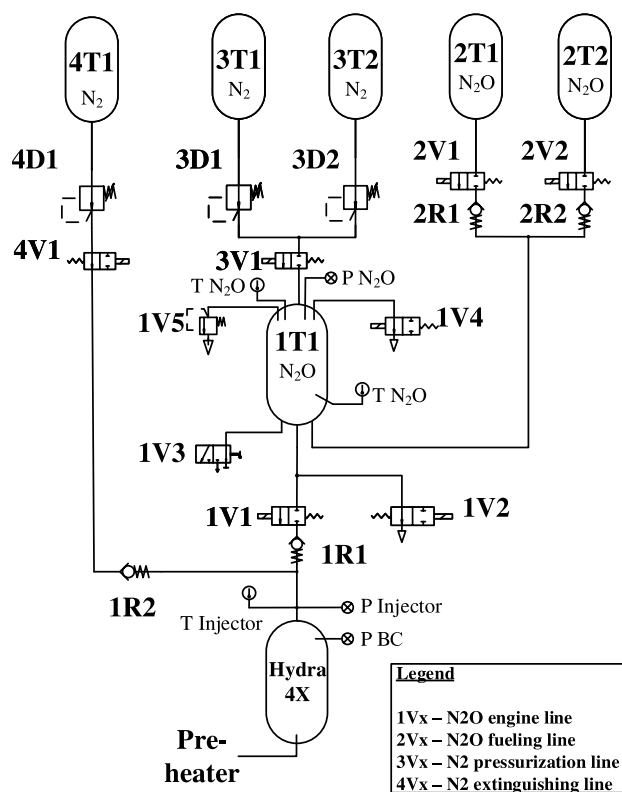
(a) PID
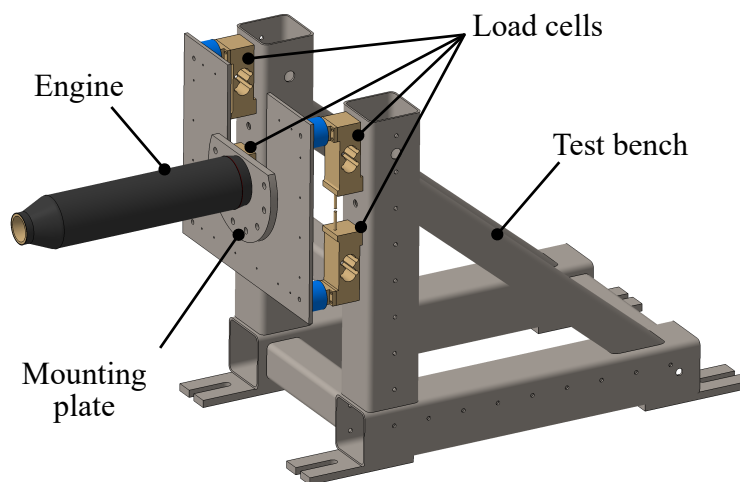
(b) Engine test bench

Figure 5. (a) Fluid plan of the fluid supply system, (b) Engine test bench with engine HYDRA 4X.

flows. Therefore, the achieved oxidizer mass flow decreases over burn time in every test, i.e. initial and end values are in a range of 10% deviation of mean oxidizer mass flow over burn time. Tank and injector pressure differ by a small value that complies with pressure loss in the feeding line. Injector and chamber pressure show increased values after opening of the main valve. After closure of the main valve, thrust and combustion chamber pressure decrease fast to values prior to ignition, while the intermediate tank pressure increases again. The injector pressure does not drop to ambient pressure again, because the feeding line is still pressurized. For the first two tests, the feeding line extends

with about 2 m length between main valve and engine, cf. Figure 5a. Due to this, the engine receives oxidizer for a longer time than desired after main valve closure. To reduce this effect, the main valve is relocated directly in front of the engine for the third and fourth test.
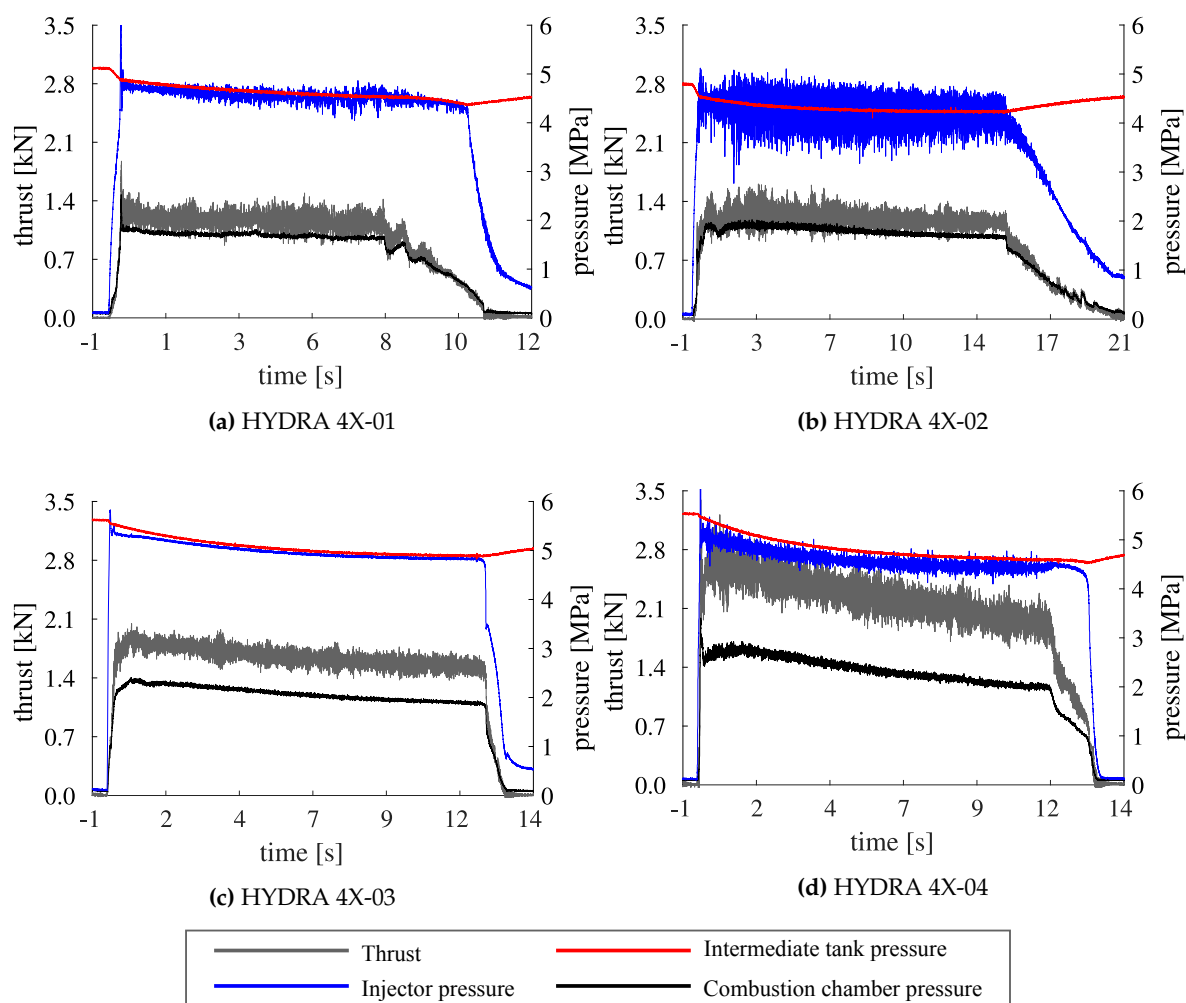

**Figure 6.** Engine test data for HYDRA 4X-01 (a), 4X-02 (b), 4X-03 (c) and 4X-04 (d).

The mean thrust of the first two engine tests is about 1.2 kN which is apparently lower than design thrust. Accordingly, the average combustion chamber pressure of 1.8 MPa is low compared to the design value of 2.5 MPa. Analysis of test parameters yields that the target value for oxidizer mass flow was not reached, and the nozzle was manufactured inaccurately. Design changes between HYDRA 4X versions 01 and 02 have been made to increase engine performance: Nozzle manufacturing was improved, post combustion chamber length was increased by 30%, and injector design was changed to improve mass flow through an increase of orifice number and manufacturing quality, and combustion of both propellants by flattening the diverting cone angle. Since there are no remarkable changes between performance results of HYDRA 4X-01 and 4X-02, the consumption of the star-shaped solid propellant grain was examined for the second test in Figure 7b. Two main aspects can be determined. First of all, it is evident that HTPB consumption decreases with combustion chamber length. The mean consumption shows values between 30 mm at the fuel grain front and only 20 mm at the end considering the star peaks. This is also apparent for star indentations where consumption values vary from 7 mm to 0 mm. Latter means no consumption at all. Hence, the consumption of star indentations is significantly lower than that of star peaks. The authors assume, that although the target mean regression rate was reached, the uneven consumption over length and major differences between star peaks and indentations contributed to engine performance, as the overall fuel grain surface in the

combustion process was decreased.

As a result, the fuel grain geometry was changed for the test of HYDRA 4X-03 as is presented in Figure 7a. The number of star peaks was decreased from 8 to 6 and the geometry was changed so that consumption of star indentations is augmented. The consumption measurements of HYDRA 4X-03 show that the design changes enhanced the HTPB consumption, especially for star indentations, as can be seen in Figure 7c. Additionally, a more even consumption along engine length was demonstrated. Therefore, a higher mean thrust value of about 1.6 kN at a chamber pressure of 2 MPa could be reached, as presented in Figure 6c. These values are still below design parameters, which can be traced back to a low oxidizer mass flow. As a result, the injector was adapted once more between tests 03 and 04 by increasing number of injecting orifices.
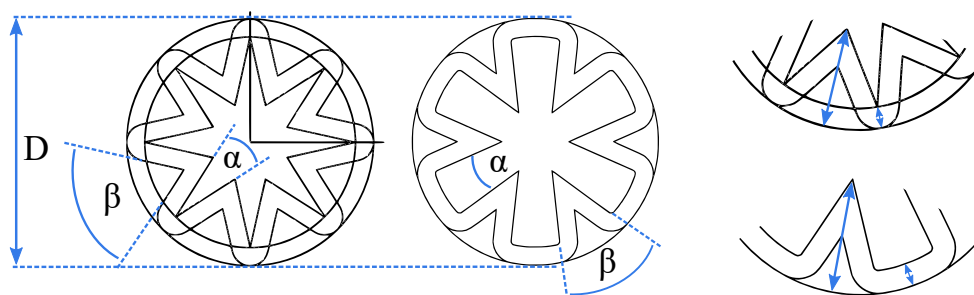
(a) Comparison of fuel grain geometries v1 (left) used in H4X-01 and H4X-02, and v2 (middle) used in H4X-03 and H4X-04. Measurement points for geometric consumption are indicated in the respective geometries on the right.
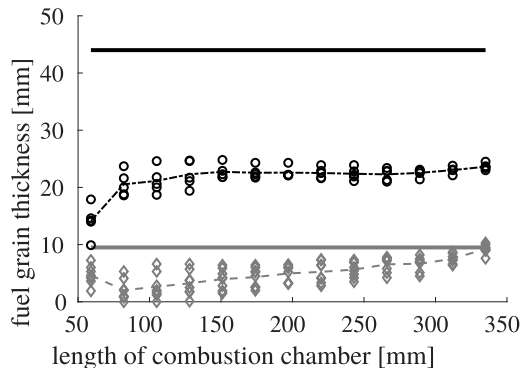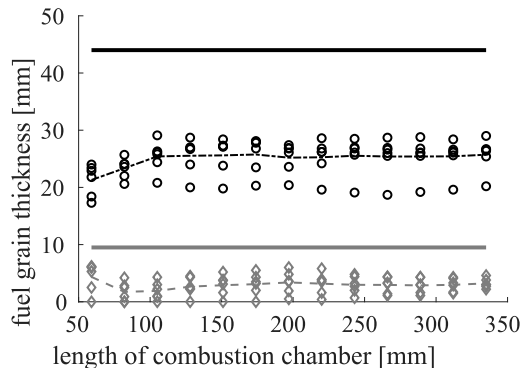
(b) HYDRA 4X-02   **(c)** HYDRA 4X-03

Figure 7. Thickness of HTPB fuel grain at star peaks in black and indentations in grey before (-) and after (- -) test, distances were measured originating from chamber wall. Symbols represent measurement points as indicated in **(a)** and lines resemble the corresponding mean values.

Table 6. Parameters of two fuel grain geometry of HYDRA 4X

	H4X-01, 02	H4X-03, 04
D	130 mm	
n	8	6
α	25°	12°
β	70°	48°

With this adjustment a mean thrust of approximately 2.3 kN was reached at a chamber pressure of 2.3 MPa, an injector pressure of 4.6 MPa and an oxidizer mass flow of 1.01 kg/s, as presented in Figure 6d. However, the mean oxidizer mass flow exceeded the design value of 0.931 kg/s. This resulted in a mean O/F of 8.4 over full test time, compared to a design O/F of 7. The fuel mass flow of

0.123 kg/s is in good accordance with the design value of 0.133 kg/s. To reach an appropriate oxidizer mass flow, the number of injecting orifices have to be decreased and the directional characteristic of the injector will be changed to supply oxidizer more directly at the star indentations. To achieve this directional behavior, the injector orifices will be aligned with the angular position of the star indentations. HYDRA 4X-04 yielded 86% efficiency of the design I_{sp}. This global efficiency can be divided into 87% combustion efficiency and approximately 99% nozzle efficiency. Although the minimum design thrust was surpassed, it could only be achieved through an excess of injected oxidizer mass flow. As the flight fluid supply system would not be able to sustain this increased oxidizer mass flow for the complete burn time, further work would have to be carried out to achieve design performance at tolerable oxidizer mass flows.
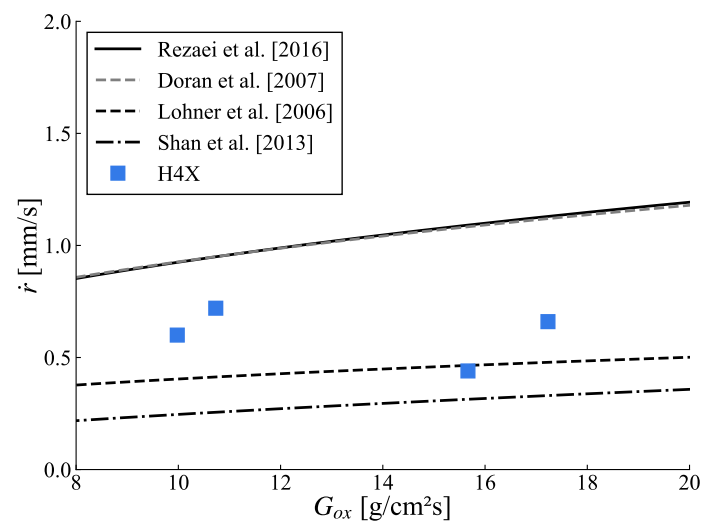

Figure 8. Comparison of fuel grain regression rates with literature data [8,31–33]

Figure 8 shows the fuel grain regression rates obtained from the four tests compared against data from literature [8,31–33]. The regression rate curves from these data follow the empirical power law [7]

$$\dot{r} = a \cdot G_{ox}^{n} \qquad (18)$$

in which the coefficients *a* and *n* are obtained through experimental data. These experiments were conducted for the same combination of propellant and oxidizer at similar combustion chamber pressures and comparable O/F. The main differences are the fuel grain geometry and injector type. Only fuel grains with single circular port geometries were tested in the references presented. The determined regression rates from four HYDRA 4X tests are located between fitting curves of [31], [32] and [8].

4.2. Impact of engine casing material on flight apogee

The different designs of two HYDRA engines 3X and 4X have already been discussed. Although there is a clear difference between engine performance data, structural changes have also been made. A comparably heavy steel casing of HYDRA 3X was replaced by a CFRP coating to reduce engine mass. This consequently results in a higher apogee. On the other hand, using CFRP also means higher effort in design, calculation, manufacturing, and costs. Therefore, it is interesting to evaluate the impact of this change on engine mass, total hybrid rocket mass, and on flight apogee. Thus, a parametric analysis for fundamental hybrid rocket pre-design is conducted. This is done by a MATLAB tool that was established during STERN II program. It uses geometric and mass relations for estimating the design of sounding rockets. The tool calculates the engine data, such as propellant mass, mass flow

and burn time, based on a requested mean thrust and total impulse. The regression rate is assumed to be constant over burn time. The fuel mass flow is calculated according to a mean fuel grain surface and a constant oxidizer mass flow. The selectable fuel grain geometry is either a monoport or a star shape and a conical nozzle is used. Two pressure tanks made from CFRP for oxidizer and pressure gas are calculated based on engine data. Residual rocket components like electronics or parachutes are estimated by the user. Physical relations for hybrid engines and flight mechanics (described in [1], [7] and [34]) are used to estimate flight performance, using the mean thrust as a constant thrust profile over burn time. The tool analyzes first estimations on rocket design factors like engine performance, geometric dimensions, and flight parameters, such as flight apogee. The analysis is suited for rockets in an impulse range of 10 to 50 kNs and cell diameters of 100 to 180 mm. A parametric study is carried out for a basic rocket design with a constant cell diameter of 150 mm while the total impulse is increased continuously from 10 to 50 kNs. The rocket engine gets larger (as more fuel is required) and longer. The engine structure mass and casing mass rise with increasing total impulse. The total impulse of an engine can be calculated by thrust F and engine burn time t_b [1] according to Equation 19. This relation can be used here, since the design tool uses a mean thrust value for calculations, even though the thrust profile is usually not constant for HRE.

$$I_{tot} = F \cdot t_b \tag{19}$$

The launch acceleration of the rocket shall be about 5 g at a rail length of 9 m. This results in a minimum thrust for an estimated rocket mass and a corresponding burn time. To characterize the relation between fuel and engine structure mass, two mass factors are introduced. Firstly, the relation factor f_{cm} compares engine casing mass m_{cas} to fuel mass m_f that can be accommodated by the engine. This factor shows how much casing mass is required for a defined fuel mass to reach a certain total impulse.

$$f_{cm} = \frac{m_{cas} + m_f}{m_f} \tag{20}$$

A second relation factor f_{em} is defined, which represents a comparison between overall engine mass m_e (including fuel mass) and fuel mass. This factor links fuel mass to engine structure mass m_{str} that includes casing and other structural engine components.

$$f_{em} = \frac{m_e}{m_f} = \frac{m_{str} + m_f}{m_f} \tag{21}$$

Using these engine parameters, a basic rocket design is developed and the results are discussed. They are compared to the design parameters of the engine HYDRA 4X for Faust II rocket that has been presented. Figure 9a shows the defined mass relation factors as a function of total impulse in a range from 10 to 50 kNs.

Two main aspects can be derived from Figure 9a. A steel casing is heavier than a CFRP casing but the relations between casing mass and fuel mass (f_{cm}) change over the total impulse range. For smaller engines with a low total impulse of about 10 kNs, the weight of a steel casing is seven times higher than the respective fuel mass. This relation decreases with total impulse and shows a factor of about 3.5 for engines with a total impulse of 50 kNs. In comparison to that, f_{cm} for a CFRP casing is nearly constant over the impulse range, where a mass factor of about 1.4 is reached. A second aspect addresses the total engine structure mass. It is derived from the casing (outer structure) and other structural components as presented. As Figure 9a shows for small engines (10 kNs), the mass factor for overall engine mass f_{em} is at 15.7 for steel and 8.8 for CFRP casing material. This shows that the residual engine structure mass (disregarding the casing) cannot be neglected, although the mass factor f_{em} decreases with rising total impulse. The overall engine structure mass with a steel casing is about 4 times higher than the required fuel mass at an impulse of 50 kNs. In contrast, the structure mass with a CFRP casing is about twice as high as the accommodated fuel mass. Thus, the data shows that the engine structure mass is
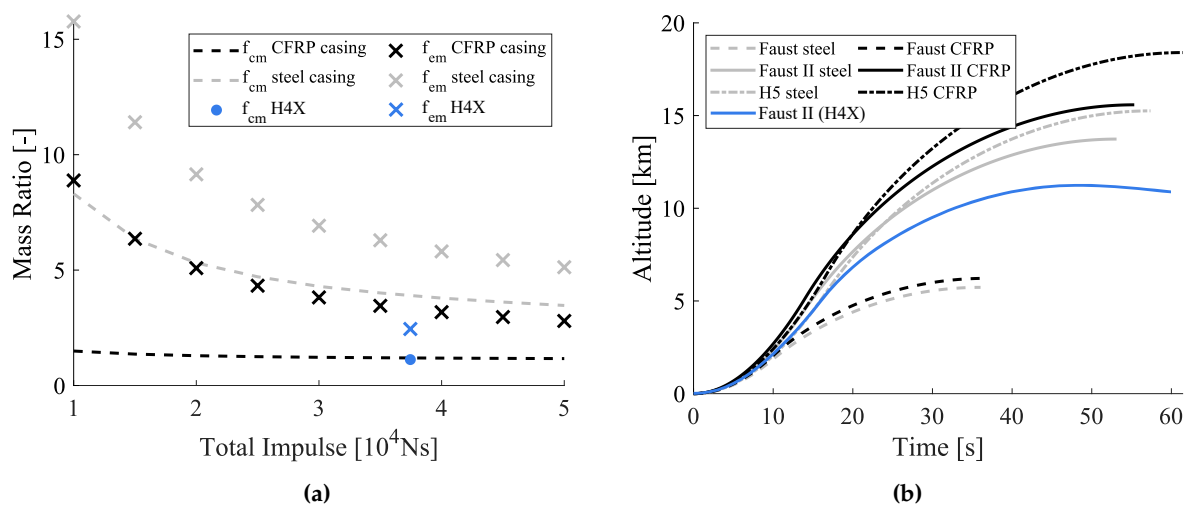
Figure 9. (a) Mass ratios f_{cm} and f_{em} for steel and CFRP casing materials. (b) Flight trajectories until apogee altitude for three different rocket designs again with steel or CFRP casing material.

relatively high compared to required fuel mass, especially, for a small impulse class. Less structure mass is needed relative to fuel mass for higher impulses. When using CFRP instead of a steel casing, the engine structure mass can be reduced by about 50 % for the whole impulse range. The mass factor f_{cm} for a steel casing shows a maximum for a small engine class, where the engine structure mass is very high compared to the fuel mass. Both mass factors decrease with increasing impulse. However, an engine with steel casing results in a mass twice as high as an engine with CFRP casing over the whole impulse range. The achieved values for the engine HYDRA 4X (35.5 kNs) are added in blue color. A f_{cm} value of 1.12 is in good accordance with the results of the parametric analysis. The engine mass factor f_{em} of 2.45 is lower than the analysis result of 3.3, which means that less structure mass is needed for this engine than the parametric tool assumes.

Figure 9b shows the effect of casing material on flight apogee. Two existing (H3X, H4X) and one theoretical (H5) engine and subsequent rocket designs are presented in two versions: Steel and CFRP, as presented in Table 7, where hybrid engine rockets for a range of impulses and rocket diameters are compared. For these designs, an approximated flight apogee is calculated to evaluate the casing mass impact. The flight trajectory is plotted until apogee where the recovery system would be activated.

Table 7. Comparison of rocket design parameters for three different engines with two different casing materials. Results presented in (..) correspond to real flight data for Faust and CAD data for Faust II.

Parameter	Faust	Faust II	H5 rocket
Cell diameter [m]	0.123	0.143	0.17
Engine	HYDRA 3X	HYDRA 4X	HYDRA 5
Thrust [kN]	1.25	2.25	3
Total Impulse [kNs]	12.50	35.55	50
Rocket mass [kg]	Steel: 26.4 (24.1) CFRP: 24.2	Steel: 44.3 CFRP: 39.6 (46.3)	Steel: 59.0 CFRP: 51.1
Apogee altitude [km]	Steel: 5.73 (5.41) CFRP: 6.22	Steel: 13.7 CFRP: 15.6 (11.2)	Steel: 15.3 CFRP: 18.4

As Figure 9b shows, an apogee of 5.7 km for Faust with a hybrid engine using a steel casing is reached. This is similar to Faust flown in 2015 with an apogee of roughly 5.4 km. Therefore, the analysis provides reasonable results. An apogee difference for the two casing materials of about 500 m and a mass difference of about 2.2 kg were derived for Faust. A higher impact on apogee difference is observed for Faust II. Using a CFRP casing, Faust II is able to reach an altitude of 15.6 km (compared to 13.7 km when using a steel casing), which represents an apogee increase of about 14%. The fully designed Faust II with a CFRP engine shows a higher mass than the pre-design (+6.7 kg), resulting

in a lower apogee altitude of 11.2 km. The trend for an increase of apogee rises for the larger engine HYDRA 5 (cf. Table 7). By using a CFRP engine casing, an increase of 3.1 km (20.3%) is achieved compared to a steel casing. It is evident that a lighter CFRP engine casing is beneficial, especially, for engines with higher total impulse and diameter values.

5. Conclusion and outlook

The previous and current development activities of hybrid rocket engines at Technische Universität Braunschweig were examined. The design of the rocket engine HYDRA 3X was described, which was launched at the Esrange Space Center in 2015. It is a hybrid engine using nitrous oxide as oxidizer and HTPB as fuel. Based on this, a new engine HYDRA 4X was developed, that is designed for the Faust II rocket. The main design changes compared to HYDRA 3X are a higher total impulse and thrust, and the CFRP casing material. Test bed and first test results of the new HYDRA 4X engine were shown. The design changes to iterate a requested engine performance were explained. In addition, the obtained fuel grain regression rates were compared to literature data.

To quantify the impact of different casing materials on rocket mass parameters, a parametric study was performed. First, casing and engine structure masses were compared to the fuel mass. It was shown that the fraction of structure mass to overall engine mass decreases over increasing total impulse, although the impact of casing material on rocket apogee altitude increases. The analysis suits best for rockets with diameters between 100 and 180 mm and impulses between 10 and 50 kNs. A CFRP engine casing material shows a clear advantage over a heavy metal casing when only flight altitude is considered. However, other design, manufacturing, and cost parameters have to be taken into account to quantify the benefit of the material choice. In a next step, the parametric analysis will be extended to a wider range of impulses and the pre-design of other rocket components like recovery and electronics system will be refined.

Author Contributions: Conceptualization, F.H. and R.S.; investigation, R.S., L.K. and F.H.; data curation, L.K and R.S.; writing–original draft preparation, F.H. and L.K.; writing–review and editing, L.K., R.S. and E.S.; visualization, L.K. and F.H.; supervision, F.H.; project administration, E.S.

Conflicts of Interest: The authors declare no conflict of interest.

Abbreviations

The following abbreviations are used in this manuscript:

Nomenclature

A	Area (unit: m^2)
a	Regression rate coefficient
C	Coefficient (unit: -)
d	Diameter (unit: m)
F	Thrust (unit: N)
G	Oxidizer mass flow to free port area ratio (unit: g/cm^{2}s)
f	Relation factor (unit: -)
I_{sp}	Specific Impulse (unit: m/s)
I_{tot}	Total Impulse (unit: Ns)
M	Molar mass (unit: g/mol)
m	Mass (unit: kg)
$\dot{m}$	Mass flow (unit: kg/s)
n	Regression rate coefficient, number (unit: -)
p	Pressure (unit: Pa)
$\dot{Q}$	Volume flow (unit: m^3/s)

R_∞	Molar gas constant (unit: J/mol·K)
T	Thermodynamic temperature (unit: K)
t	Time (unit: s)

Greek Symbols

η	Efficiency (unit: -)
Γ	Auxiliary function (unit: -)
γ	Ratio of specific heats (unit: -)
ρ	Density (unit: kg/m^3)

Subscripts

a	Ambient
b	Burn
cas	Casing
c	Chamber
D	Discharge
e	Engine, Exit (Nozzle)
f	Fuel
ox	Oxidizer
p	Port
str	Structure
t	Throat
th	Theoretical

Abbreviations

TRL	Technical readiness level
HRE	Hybrid Rocket Engine
DLR	German Aerospace Center
STERN	Studentische Experimental-Raketen
MORABA	Mobile Raketenbasis
IRAS	Institute of Space Systems
ERIG	ExperimentalRaumfahrt-InteressenGemeinschaft
BMWi	Federal Ministry of Economic Affairs and Energy
HYDRA	Hybrid Demonstrations-RaketenAntrieb
HTPB	Hydroxyl-terminated polybutadiene
N_2O	Nitrous oxide
H_2O_2	Hydrogen peroxide
LDPE	Low density polyethylene
PE	polyethylene
LOX	Liquid oxygen
CFRP	carbon fiber reinforced plastic
O/F	Oxidizer to fuel mass ratio
NASA	National Aeronautics and Space Administration
CEA	Chemical Equilibrium with Applications
PID	Piping and Instrumentation Diagram

References

1. Sutton, G.; Biblarz, O. *Rocket Propulsion Elements*, 7 ed.; John Wiley and Sons, Inc., 2001. pp. 27-38, 62-68, 77-82, 580.

2. Li, X.; Tian, H.; Yu, N.; Cai, G. Experimental investigation of fuel regression rate in a HTPB based lab-scale hybrid rocket motor. *Acta Astronautica* **2014**, *105*, 95–100.

3. Mazzetti, A.; Merotto, L.; Pinarello, G. Paraffin-based hybrid rocket engines applications: A review and a market perspective. *Acta Astronautica* **2016**, *Vol. 126*, 286–297.

4. Schmierer, C.; Kobald, M.; Fischer, U.; Tomilin, K.; Petrarolo, A.; Hertel, F. Advancing Europe's Hybrid Rocket Engine Technology with Paraffin and LOX. *8th European Conference for Aeronautics and Aerospace Sciences (EUCASS)* **2019**.

5. Schmierer, C. Analysis of a Hybrid Propulsion Lunar Sample Return Mission. PhD thesis, University of Stuttgart, 2019.

6. Schmucker, R.H. *Hybridraketenantriebe*; Wilhelm Goldmann Verlag GmbH, 1972. pp. 22-24, 67-70.

7. Barrère, M.; Schneider, W.K.; Roy, M.; Von Kármán, T. *Raketenantriebe*; Elsevier Publishing Co., 1961. pp. 66-72, 98, 112-114.

8. Rezaei, H.; Soltani, M.R.; Mohammadi, A.R. Experimental Study of Fuel Regression Rate in a HTPB/N2O Hybrid Rocket Motor. *Scientia Iranica* **2018**, *25*, 253–265. doi:10.24200/sci.2017.4317.

9. Chiaverini, M.J.; Kuo, K.K.; Peretz, A.; Harting, G. Regression-Rate and Heat-Transfer Correlations for Hybrid Rocket Combustion. *Journal of Propulsion and Power* **2001**, *Vol. 17, No. 1*.

10. Carmicino, C.; Scaramuzzino, F.; Sorge, A.R. Trade-off between paraffin-based and aluminium-loaded HTPB fuels to improve performance of hybrid rocket fed with N2O. *Aerospace Science and Technology* **2014**, *Vol. 37*, 81–92.

11. Sun, X.; Tian, H.; Li, Y.; Yu, N.; Cai, G. Regression rate behaviors of HTPB-based propellant combinations for hybrid rocket motor. *Acta Astronautica* **2016**, *Vol. 119*, 137–146.

12. Cheng, P.; Lia, Q.; Chen, H. Flow characteristics of a pintle injector element. *Acta Astronautica* **2019**, *Vol. 154*, 61–66.

13. Di Martino, G.D.; Malgieri, P.; Carmicino, C.; Savino, R. A simplified computational fluid-dynamic approach to the oxidizer injector design in hybrid rockets. *Acta Astronautica* **2019**, *Vol. 129*, 8–21.

14. Greatrix, D.R. Regression rate estimation for standard-flow hybrid rocket engines. *Aerospace Science and Technology* **2009**, *Vol. 13*, 358–363.

15. Hui, T.; Yijie, L.; Peng, Z. Transient simulation of regression rate on thrust regulation process in hybrid rocket motor. *Chinese Journal of Aeronautics* **2014**, *Vol. 27(6)*, 1343–1351.

16. Chiba, K.; Kanzaki, M.; Nakamiya, M.; Kitagawa, K.; Shimada, T. Conceptual Design of Single-Stage Launch Vehicle with Hybrid Rocket Engine for Scientific Observation Using Design Informatics. *Journal of Space Engineering* **2013**, *Vol. 6, No. 1*.

17. Bozic, O.; Poppe, G.; Porrmann, D. An advanced hybrid rocket engine for an alternative upper stage of the Brazilian VLM 1 LEO-launcher. *65th International Aeronautics Congress* **2013**.

18. Karp, A.; Benito, J.; Nakazono, B.; Kim, H.; Shotwell, R.; Brandeau, E.; Vaughan, D.; Story, G. A Hybrid Mars Ascent Vehicle Design and FY 2016 Technology Development. *IEEE Aerospace Conference* **2017**.

19. Tsohas, J.; Appel, B.; Rettenmaier, A.; Walker, M.; Heister, S.D. Development and Launch of the Purdue Hybrid Rocket Technology Demonstrator. *45th AIAA/ASME/SAE/ASEE Joint Propulsion Conference* **2009**.

20. Kawai, H.; Harada, J.; Oguro, J.; Banno, A.; I., N. Launches of Hybrid Rockets with Wax Fuel. *49th AIAA/ASME/SAE/ASEE Joint Propulsion Conference* **2013**.

21. Werner, R.; Knop, T.; Wink, J.; Ehlen, J.; Huijsman, R.; Powell, S.; Florea, R.; Wieling, W.; Cervone, A.; Zandbergen, B. Development and Performance of the 10 kN Hybrid Rocket Motor for the Stratos II Sounding Rocket. *Space Propulsion* **2016**.

22. DLR-Raumfahrtmanagement. *STERN: Studentische Experimental-Raketen*, 2012 (accessed on 13-01-2020). Available online: https://www.dlr.de/rd/PortalData/28/Resources/dokumente/rl/STERN_Flyer.pdf.

23. Becker, J.; Grefen, B.; Stoll, E. Results of the Leonis Project and Launch Campaign within the STERN Program. *Deutscher Luft- und Raumfahrtkongress* **2016**.

24. Schuettauf, K.; Stamminger, A.; Lappoehn, K. The STERN Project - Hand On Rockets Science for University Student **2016**.

25. Rothe, D.; Hink, R. Faust Hybrid Rocket - Current Status. *Deutscher Luft- und Raumfahrtkongress* **2015**.

26. Dullo, C.M.U.; Hink, R. Experimental Analyses of the HTPB-Aluminum Mixtures for Hybrid Rocket Engines. *Deutscher Luft- und Raumfahrtkongress* **2013**.

27. Gamper, E.; Hink, R. Design and Test of Nitrous Oxide Injectors for a Hybrid Rocket Engine. *Deutscher Luft- und Raumfahrtkongress* **2015**.

28. Baade, M.; Hink, R. Design of a Nozzle for a Hybrid Rocket Engine Using an Explicit Finite-Volume Based Simulation for Heat Transfer. *Deutscher Luft- und Raumfahrtkongress* **2013**.

29. Hink, R. HYDRA 3 Hybrid Rocket Engine – Flight Version Test Results. *Deutscher Luft- und Raumfahrtkongress* **2015**.

30. Lemmon, E.W.; McLinden, M.O.; Friend, D.G. *NIST Chemistry WebBook, NIST Standard Reference Database Number 69*; National Institute of Standards and Technology; chapter Thermophysical Properties of Fluid Systems.

31. Lohner, K.; Dyer, J.; Doran, E.; Dunn, Z.; Zilliac, G., Fuel Regression Rate Characterization Using a Laboratory Scale Nitrous Oxide Hybrid Propulsion System. In *42nd AIAA/ASME/SAE/ASEE Joint Propulsion Conference*. doi:10.2514/6.2006-4671.

32. Doran, E.; Dyer, J.; Lohner, K.; Dunn, Z.; Cantwell, B.; Zilliac, G., Nitrous Oxide Hybrid Rocket Motor Fuel Regression Rate Characterization.   In *43rd AIAA/ASME/SAE/ASEE Joint Propulsion Conference*. doi:10.2514/6.2007-5352.

33. Shan, F.; Hou, L.; Piao, Y. Combustion performance and scale effect from N2O/HTPB hybrid rocket motor simulations. *Acta Astronautica* **2013**, *85*, 1 – 11. doi:https://doi.org/10.1016/j.actaastro.2012.12.013.

34. Andrea, L. *A Mathematical Perspective on Flight Dynamics and Control*; Springer, 2017.